Supporting Information for Spherical convolutions on molecular graphs for protein model quality assessment

Ilia Igashov*
Moscow Institute of Physics and Technology
Univ. Grenoble Alpes, Inria, CNRS,
Grenoble INP, LJK, 38000 Grenoble, France
igashov.is@phystech.edu

Nikita Pavlichenko*
Moscow Institute of Physics and Technology
Dolgoprudny, Moscow region, 141700, Russia
pavlichenko.nv@phystech.edu

Sergei Grudinin
Univ. Grenoble Alpes, Inria, CNRS, Grenoble INP, LJK, 38000 Grenoble, France
sergei.grudinin@inria.fr

1 Real spherical harmonics

As we mention in the main text, a *real* function on a unit sphere $f(\theta, \varphi)$ can be decomposed in a polynomial basis more compactly using only *real spherical harmonics*. This can be easily demonstrated using the fact that the real function and its conjugate must be equal to each other. There are multiple definitions of real spherical harmonics. The most accepted one is the classical orthonormal version,

$$Y_l^m = \begin{cases} \sqrt{2}(-1)^m \operatorname{Im}\left[Y_l^{|m|}\right] & \text{if } m < 0 \\ Y_l^0 & m = 0 \\ \sqrt{2}(-1)^m \operatorname{Re}\left[Y_l^m\right] & \text{if } m > 0. \end{cases} \tag{1}$$

In our source code, however, by default we stick to a different definition,

$$Y_l^m = \begin{cases} -2 \operatorname{Im}\left[Y_l^{|m|}\right] & \text{if } m < 0 \\ Y_l^0 & m = 0 \\ 2 \operatorname{Re}\left[Y_l^m\right] & \text{if } m > 0. \end{cases} \tag{2}$$

2 Spherical convolution with the radial part

We have also conducted experiments using 3D polynomial representations of our molecular graphs. Let us consider a complex square-integrable matrix function $\boldsymbol{F}(r, \theta, \varphi)$ defined in $\mathbb{R}^3$. This function can be expanded in a polynomial basis using spherical harmonics as the angular basis functions and classical orthogonal polynomials for the radial part,

$$\boldsymbol{F}(r, \theta, \varphi) = \sum_{n=0}^{\infty} \sum_{l=0}^{n} \sum_{m=-l}^{l} \boldsymbol{W}_{nlm} R_n^l(r) Y_l^m(\theta, \varphi), \tag{3}$$

*These authors contributed equally.

Preprint.

where $\boldsymbol{W}_{nlm}$ are the expansion coefficients, $R_n^l(r)$ are the radial polynomials, and $Y_l^m(\theta, \varphi)$ are the spherical harmonics. In order to use such functions defined in $\mathbb{R}^3$ as trainable filters, we do the following.

As we describe in Section 3.1 of the main text, a protein graph $\mathcal{G}$ is constructed on Voronoi 3D-tessellation of the protein model, and edges of the graph $\mathcal{G}$ are associated with the pairs of residues whose Voronoi cells have a non-zero contact surface. Let $\boldsymbol{S}$ be a symmetric *weighted* adjacency matrix of the graph $\mathcal{G}$, such that an entry s_{uv} of the matrix $\boldsymbol{S}$ equals to an area of the contact surface between Voronoi cells of the residues u and v. We consider these contact areas between the nodes as the strength of the *interactions* between the respective residues. This allows us to simplify the original polynomial representation (4).

More precisely, we approximate the expansion (4) of the function $\boldsymbol{F}$ by cutting the series at the maximum expansion order L and assuming the radial part as an independent multiplier $g(r)$, where g is an arbitrary function,

$$\boldsymbol{F}(r, \theta, \varphi) \approx \hat{\boldsymbol{F}}(r, \theta, \varphi) = g(r) \sum_{l=0}^{L} \sum_{m=-l}^{l} \boldsymbol{W}_l^m Y_l^m(\theta, \varphi). \tag{4}$$

Hence, the convolution operation can be written as follows,

$$\boldsymbol{F} \circ v = \sum_{u \in \mathcal{N}(v)} \hat{\boldsymbol{F}}(s_{uv}, \theta_v^u, \varphi_v^u) \boldsymbol{x}_v. \tag{5}$$

In this work, we put

$$g(\boldsymbol{S}) \equiv \hat{\boldsymbol{S}} \equiv \boldsymbol{D}^{-1/2} \boldsymbol{S} \boldsymbol{D}^{-1/2}, \tag{6}$$

where $\boldsymbol{D}$ is a diagonal matrix of the nodes' degrees, and thus the kth convolution layer in the network can be written down in the following form,

$$\boldsymbol{H}^k = \sigma \left(\sum_{l,m}^{L} \hat{\boldsymbol{S}} \odot Y_l^m(\boldsymbol{A}_\Omega) \boldsymbol{H}^{k-1} \boldsymbol{W}_l^m + \boldsymbol{H}^{k-1} \boldsymbol{W} + \boldsymbol{b} \right), \tag{7}$$

where the operation $\odot$ is the elementwise multiplication.

3 Baseline experiments

Our experiments have demonstrated that the spherical networks significantly outperform the baseline architectures. To prove that this difference is not the result of not optimally chosen parameters or a non-optimal design of the baseline networks, we have carried out several studies on grid-search of network architectures' parameters.

As we have mentioned in Section 4.3 of the main text, we define our baseline GCN networks by three parameters. These are the number of the encoder, the message-passing, and the scorer layers. We varied each of these parameters in the following ranges, encoder – $[0, 3]$, message-passing – $[6, 8]$, scorer – $[0, 3]$.

We then selected the best network architectures based on per-residue Pearson's correlation coefficient, since it is the most similar metric to the Mean Squared Error, which is our loss function.

Figure S1 shows the results of the grid search. It is clear that the best results can be obtained with the maximum values of the encoder and the message-passing sizes. For the number of the scorer layers, we can not confidently comment on the type of dependence, so we simply chose the best network based on the performed experiments. If we add more layers, especially to the encoder part, we see a significant growth of the number of trainable parameters and the training time. Therefore, we chose the best network parameters $(3, 8, 3)$ as the baseline architecture.

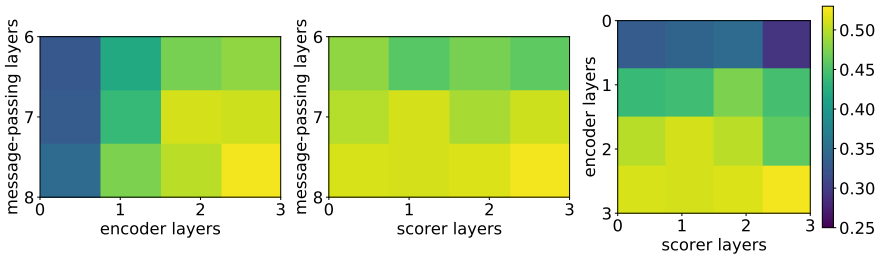

Figure S1: Heat map representation of the maximum per-residue Pearson's correlation coefficients achieved with different numbers of the encoder, message-passing, and scorer layers of the baseline networks.

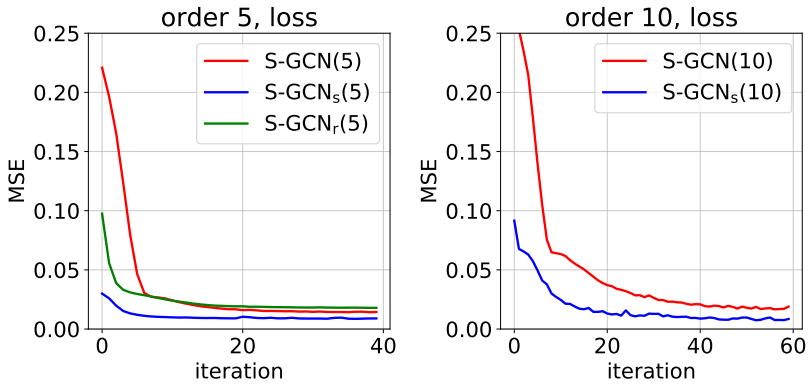

Figure S2: Training loss of networks S-GCN(5), S-GCN$_s$(5), S-GCN$_r$(5) (left) ans S-GCN(10), S-GCN$_s$(10) (right).

4 Spherical convolutional networks experiments

As we have mentioned in Section 4.4 of the main text, we experimented with different configurations of S-GCNs. First of all, we tried different expansion orders of spherical harmonics: 3, 5, 7 and 10. For each of the expansion orders, we used the grid-search technique to find optimal values of hyperparameters, which are the dropout probability and the L_2-regularization coefficient. For the dropout probability, we iterated through the values $\{0.05, 0.1, 0.2, 0.3, 0.4\}$. For the regularization coefficient, we iterated through the values $\{0.001, 0.005, 0.01, 0.05, 0.1, 0.5\}$.

Besides the choice of optimal hyperparameters, at the beginning of our studies we also experimented with different architectures for S-GCN(5). We started with three spherical layers without dropout and batch normalization layers, and after multiple transformations we finally settled upon the architecture proposed in Table 1 of the main text. After adding three linear layers to the end of S-GCN, we obtained our second architecture S-GCN$_s$. We did not perform the search of hyperparameters with S-GCN$_s$, but we experimented with multiple architectures as well.

We also trained networks S-GCN$_r$ that contain convolution layers (7) with the radial component. However, they did not demonstrate improvements over other S-GCNs architectures.

Figure S2 shows training trajectories of the loss function for networks S-GCN(5), S-GCN$_s$(5), S-GCN$_r$(5), S-GCN(10) and S-GCN$_s$(10). Figures S3 and S4 show training trajectories of the MSE, R^2 and correlations obtained on the validation CASP12 dataset for networks S-GCN(5), S-GCN$_s$(5), S-GCN$_r$(5), S-GCN(10) and S-GCN$_s$(10). Each of these metrics was computed for local and global predictions in the global and per-target modes. Figure S5 shows training trajectories of z-score and rank metrics obtained on the validation CASP12 dataset for networks S-GCN(5), S-GCN$_s$(5), S-GCN$_r$(5), S-GCN(10) and S-GCN$_s$(10).

5 Data

To train, validate and test our networks we used server submissions from the previous CASP (Critical Assessment of protein Structure Prediction) challenges. For training, we used models from stage-2 server submissions of CASP[8-11], we validated the performance of our networks on CASP12, and then tested them on raw (unprocessed) data from CASP[12-13]. Tables S5-S7 list all the targets and the corresponding number of models.

Following previous studies [1, 2], we pruned the training dataset and kept only 3D models of proteins that have meaningful physics of interactions. For training, we kept only protein targets of water-soluble proteins in a physiologically monomeric state. Additionally, we excluded models with missing residues with respect to the target protein structures.

Following previous studies [3, 2], we have also augmented the training set with protein models generated as local perturbations of the target structures. To do so, we followed the previously published protocols, and used the normal mode analysis method NOLB [4]. On average, we generated about 50 additional *near-native* models per target.

We also normalized features corresponding to the cell volume, cell solvent-accessible surface area, and graph node 'buriedness' within each model. For the architecture S-GCN$_\mathrm{r}$, the weighted adjacency matrix $\boldsymbol{S}$ was normalized according to eq. (6).

6 Evaluation details

6.1 Metrics

The loss function of our networks is a Mean Squared Error between predicted and ground-truth local CAD-scores of all the residues in the protein models. Thus, we should expect the performance of our method to be optimized with respect to different correlation metrics. However, the main evaluation criterion of model quality assessment methods in CASP is the sum of (filtered) z-scores. More precisely, this is a metric that demonstrates how well a method can select the best available protein models, and also it normalizes the score by the "difficulty" of the models. The z-scores are computed in the following way. Firstly, for each target we collect a model with the highest predicted global score. After, for all the models within a target, we calculate the mean ground-truth score, which is the mean of its global CAD-scores, and also the standard deviation of these scores. Then, for each of the top-1 predictions, we evaluate the difference between its ground-truth score and the mean within the target, divided by the corresponding standard deviation. Finally, we sum up all the top-1 z-scores – and this is precisely the main metric for the evaluation of CASP structure prediction and model quality assessment methods. In some cases, the CASP evaluators filter out outliers and recompute the final statistics.

6.2 Bootstrapping

To evaluate the mean and variance of the obtained metrics, we used the bootstrap method, as it is explained below. For the per-model metrics, we took a bootstrap sample of predictions concatenated by targets and calculated metrics on this sample, then we repeated it for $B = 10^6$ times to get the precision of the order of 0.001. For the per-target metrics, we took a bootstrap sample from a set of target metrics and then aggregated these in the following way. We computed a Fisher mean of Pearson's and Spearman's correlation coefficients and averaged over the metrics. After applying these steps, we obtained distributions of the computed metrics. We can assume them normal, as it can be verified using the Shapiro–Wilk test.

Tables S1-S4 list the confidence intervals of the confidence level of 0.95 for the mean value for each metric constructed in the following way,

$$\left(\overline{X} \pm z_{0.975}\hat{\sigma}\right),$$

where $\overline{X}$ is a sample mean of metric, $\hat{\sigma}$ is a sample standard derivation, and $z_{0.975}$ is the 0.975-quantile of standard normal distribution.

Table S1: CASP13 per-model metrics.

Method	MSE	R^2	Pearson, r	Spearman, ρ
SBROD	0.0503 ± 0.0015	-3.235 ± 0.149	0.417 ± 0.021	0.433 ± 0.021
VoroMQA	0.0380 ± 0.0010	-2.198 ± 0.104	0.659 ± 0.019	0.688 ± 0.017
ProQ3	0.0353 ± 0.0012	-1.97 ± 0.132	0.726 ± 0.013	0.728 ± 0.014
Ornate	0.0095 ± 0.0003	0.192 ± 0.024	0.786 ± 0.010	0.799 ± 0.011
VoroCNN	0.0074 ± 0.0003	0.368 ± 0.024	0.764 ± 0.011	0.767 ± 0.012
Baseline	0.0167 ± 0.0006	-0.424 ± 0.046	0.465 ± 0.021	0.491 ± 0.020
S-GCN(5)	0.0131 ± 0.0004	-0.118 ± 0.033	0.806 ± 0.009	0.808 ± 0.010
S-GCN(10)	0.0068 ± 0.0002	0.422 ± 0.017	0.774 ± 0.01	0.783 ± 0.011
S-GCN$_s$(5)	0.0196 ± 0.0005	-0.668 ± 0.053	0.801 ± 0.01	0.799 ± 0.011
S-GCN$_s$(10)	0.0078 ± 0.0003	0.336 ± 0.018	0.779 ± 0.01	0.785 ± 0.011

Table S2: CASP13 per-target metrics.

Method	z-score	MSE	R^2	Pearson, r	Spearman, ρ
SBROD	1.453 ± 0.181	0.0515 ± 0.0121	-3.235 ± 0.149	0.417 ± 0.021	0.433 ± 0.021
VoroMQA	1.369 ± 0.222	0.0380 ± 0.0010	-15.931 ± 8.854	0.803 ± 0.034	0.767 ± 0.033
ProQ3	1.369 ± 0.222	0.0348 ± 0.0076	-17.519 ± 8.838	0.775 ± 0.037	0.737 ± 0.035
Ornate	1.403 ± 0.205	0.0095 ± 0.0024	-2.325 ± 1.814	0.814 ± 0.030	0.786 ± 0.029
VoroCNN	1.517 ± 0.192	0.0074 ± 0.0021	-1.961 ± 1.852	0.810 ± 0.030	0.771 ± 0.028
Baseline	0.865 ± 0.220	0.0167 ± 0.0048	-6.375 ± 4.677	0.647 ± 0.045	0.619 ± 0.043
S-GCN(5)	1.361 ± 0.202	0.0131 ± 0.0028	-3.458 ± 2.110	0.789 ± 0.032	0.743 ± 0.032
S-GCN(10)	1.247 ± 0.196	0.0068 ± 0.0015	-1.348 ± 1.028	0.721 ± 0.038	0.694 ± 0.038
S-GCN$_s$(5)	1.582 ± 0.180	0.0196 ± 0.0036	-6.415 ± 3.388	0.820 ± 0.033	0.772 ± 0.034
S-GCN$_s$(10)	1.350 ± 0.206	0.0078 ± 0.0019	-1.925 ± 1.445	0.746 ± 0.042	0.709 ± 0.041

Table S3: CASP12 per-model metrics.

Method	MSE	R^2	Pearson, r	Spearman, ρ
SBROD	0.9611 ± 0.0064	-81.935 ± 2.78	0.552 ± 0.017	0.531 ± 0.019
VoroMQA	0.0513 ± 0.0011	-3.428 ± 0.138	0.675 ± 0.016	0.700 ± 0.016
ProQ3	0.0352 ± 0.0010	-2.038 ± 0.133	0.795 ± 0.008	0.806 ± 0.009
Ornate	0.0067 ± 0.0002	0.423 ± 0.016	0.813 ± 0.009	0.805 ± 0.010
VoroCNN	0.0073 ± 0.0002	0.369 ± 0.022	0.818 ± 0.009	0.803 ± 0.010
Baseline	0.0108 ± 0.0004	0.065 ± 0.027	0.658 ± 0.014	0.666 ± 0.015
S-GCN(5)	0.0098 ± 0.0003	0.157 ± 0.025	0.854 ± 0.007	0.831 ± 0.009
S-GCN(10)	0.0049 ± 0.0001	0.573 ± 0.013	0.812 ± 0.009	0.789 ± 0.011
S-GCN$_s$(5)	0.0147 ± 0.0003	-0.272 ± 0.041	0.872 ± 0.007	0.852 ± 0.008
S-GCN$_s$(10)	0.0059 ± 0.0002	0.492 ± 0.013	0.803 ± 0.009	0.790 ± 0.011

Table S4: CASP12 per-target metrics.

Method	z-score	MSE	R^2	Pearson, r	Spearman, ρ
SBROD	1.282 ± 0.296	0.9611 ± 0.0692	-427.775 ± 99.211	0.761 ± 0.059	0.683 ± 0.059
VoroMQA	1.410 ± 0.250	0.0512 ± 0.0122	-19.762 ± 5.565	0.802 ± 0.043	0.765 ± 0.044
ProQ3	1.669 ± 0.233	0.0354 ± 0.0072	-16.570 ± 5.92	0.800 ± 0.047	0.749 ± 0.048
Ornate	1.780 ± 0.250	0.0067 ± 0.0023	-1.102 ± 0.664	0.827 ± 0.034	0.781 ± 0.035
VoroCNN	1.871 ± 0.244	0.0073 ± 0.0023	-1.381 ± 0.579	0.816 ± 0.034	0.773 ± 0.039
Baseline	1.025 ± 0.224	0.0108 ± 0.0039	-2.64 ± 1.181	0.676 ± 0.048	0.603 ± 0.047
S-GCN(5)	1.704 ± 0.281	0.0097 ± 0.0032	-1.89 ± 0.862	0.796 ± 0.041	0.737 ± 0.046
S-GCN(10)	1.665 ± 0.219	0.0049 ± 0.0012	-0.83 ± 0.446	0.709 ± 0.049	0.679 ± 0.050
S-GCN$_s$(5)	1.609 ± 0.260	0.0147 ± 0.0034	-3.866 ± 1.113	0.815 ± 0.040	0.761 ± 0.046
S-GCN$_s$(10)	1.303 ± 0.305	0.0059 ± 0.0021	-0.917 ± 0.512	0.736 ± 0.054	0.682 ± 0.051

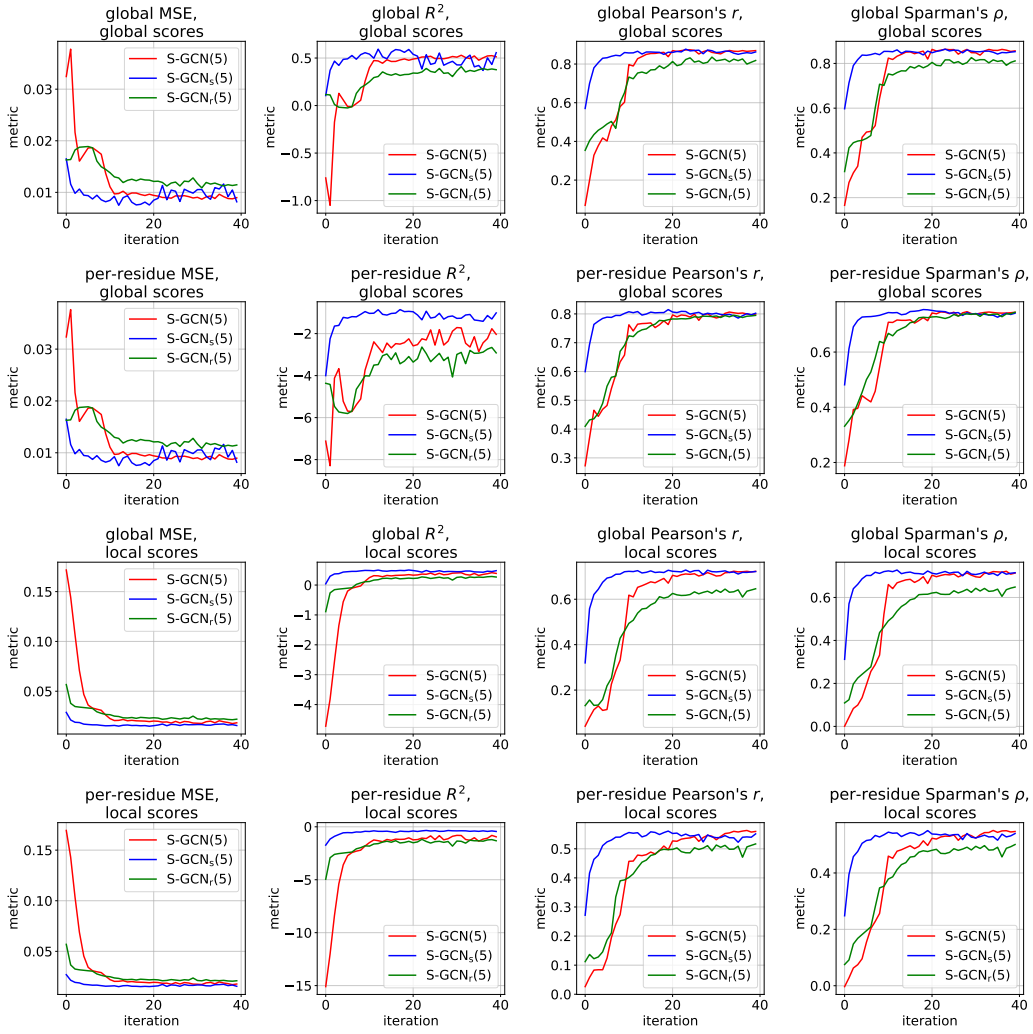

Figure S3: Training trajectories of networks S-GCN(5), S-GCN$_s$(5) and S-GCN$_r$(5) obtained on the validation CASP12 dataset. Each metric was computed for the local and global scores in the global and per-target modes.

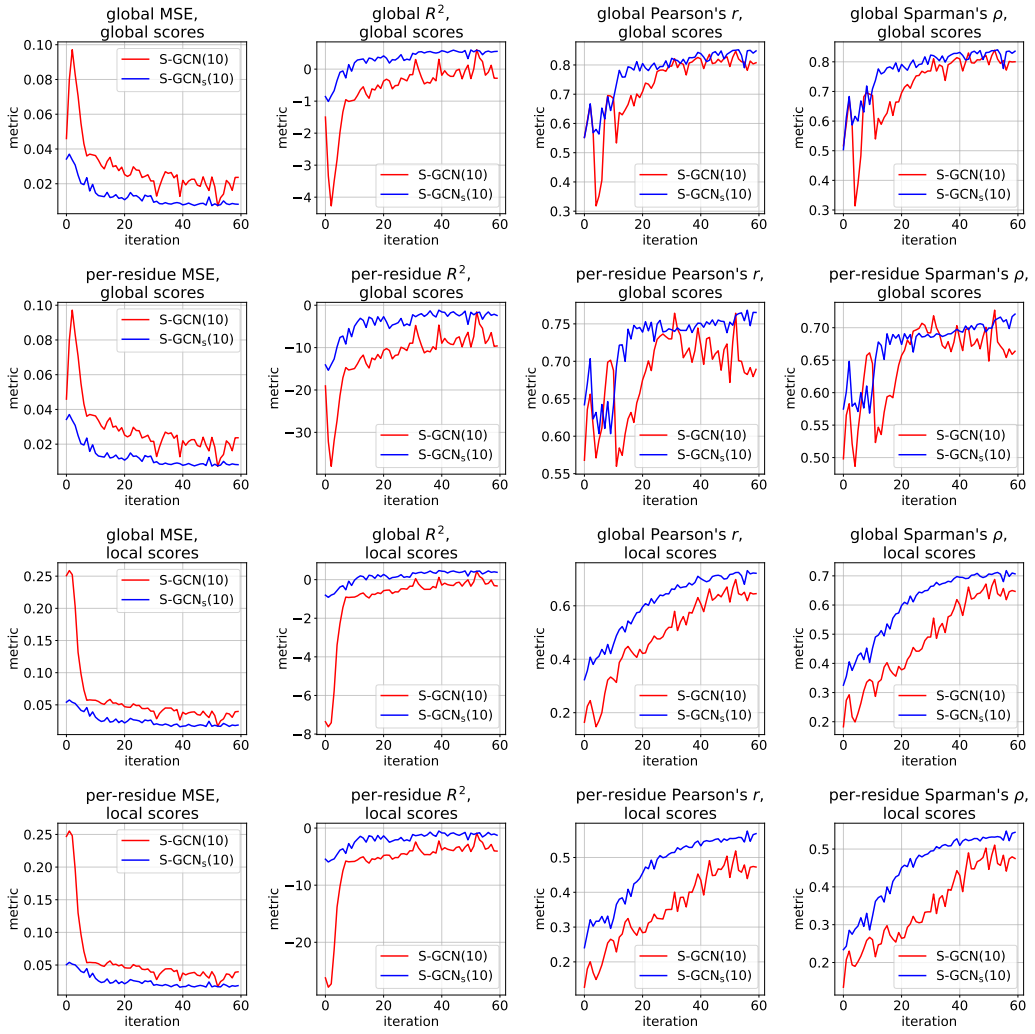

Figure S4: Training trajectories of networks S-GCN(10) and S-GCN$_s$(10) obtained on the validation CASP12 dataset. Each metric was computed for the local and global scores in the global and per-target modes.

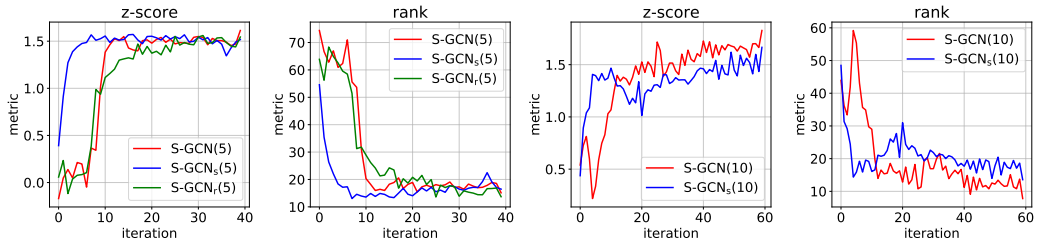

Figure S5: Trajectories of ranks and z-scores of networks S-GCN(5), S-GCN$_s$(5), S-GCN$_r$(5), S-GCN(10) and S-GCN$_s$(10) obtained on the validation CASP12 dataset.

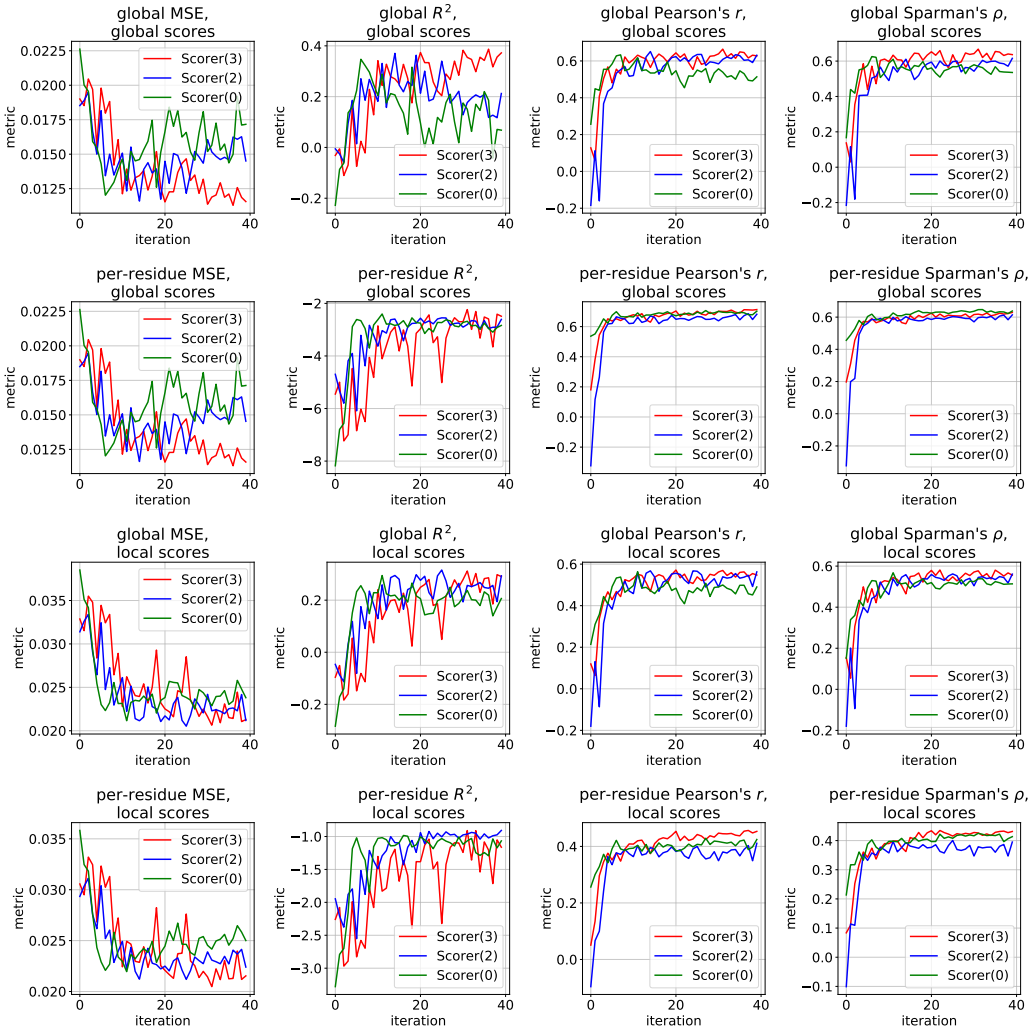

Figure S6: Training trajectories of the baseline networks with different numbers of layers in the Scorer (3, 2, 0) obtained on the validation CASP12 dataset. Each metric was computed for the local and global scores in the global and per-target modes.

Table S5: CASP targets used for training.

Dataset	Targets
CASP8 99 targets 24,414 models	T0387, T0388, T0389, T0390, T0391, T0392, T0393, T0394, T0398, T0399, T0400, T0401, T0402, T0404, T0406, T0407, T0411, T0412, T0414, T0415, T0416, T0417, T0418, T0419, T0420, T0421, T0422, T0423, T0424, T0425, T0426, T0427, T0428, T0429, T0431, T0432, T0433, T0434, T0435, T0436, T0437, T0438, T0440, T0441, T0442, T0444, T0445, T0446, T0447, T0448, T0449, T0450, T0451, T0452, T0453, T0454, T0455, T0456, T0457, T0458, T0459, T0460, T0461, T0462, T0463, T0464, T0469, T0470, T0471, T0472, T0473, T0475, T0477, T0479, T0481, T0483, T0485, T0486, T0487, T0488, T0490, T0491, T0492, T0493, T0495, T0497, T0501, T0502, T0503, T0504, T0505, T0506, T0507, T0508, T0509, T0511, T0512, T0513, T0514
CASP9 92 targets 23,674 models	T0515, T0518, T0520, T0521, T0522, T0523, T0524, T0525, T0526, T0527, T0528, T0530, T0532, T0533, T0536, T0538, T0539, T0540, T0541, T0542, T0543, T0544, T0545, T0547, T0548, T0551, T0552, T0553, T0555, T0557, T0558, T0560, T0561, T0563, T0564, T0565, T0566, T0567, T0569, T0570, T0572, T0573, T0574, T0575, T0576, T0579, T0580, T0581, T0582, T0584, T0585, T0586, T0588, T0589, T0592, T0593, T0594, T0596, T0597, T0598, T0599, T0601, T0603, T0606, T0607, T0608, T0609, T0610, T0611, T0612, T0613, T0614, T0615, T0617, T0618, T0619, T0620, T0622, T0623, T0624, T0625, T0626, T0627, T0628, T0630, T0634, T0635, T0636, T0638, T0640, T0641, T0643
CASP10 69 targets 11,541 models	T0645, T0648, T0650, T0651, T0652, T0653, T0654, T0655, T0657, T0658, T0659, T0661, T0662, T0663, T0664, T0666, T0667, T0669, T0671, T0672, T0676, T0678, T0679, T0681, T0682, T0683, T0685, T0686, T0687, T0688, T0689, T0690, T0691, T0692, T0693, T0696, T0698, T0699, T0701, T0702, T0703, T0704, T0707, T0708, T0710, T0711, T0713, T0714, T0715, T0716, T0717, T0720, T0721, T0726, T0733, T0737, T0738, T0742, T0743, T0744, T0746, T0747, T0749, T0750, T0752, T0753, T0755, T0757, T0758
CASP11 73 targets 13,789 models	T0759, T0760, T0761, T0762, T0763, T0764, T0765, T0766, T0767, T0768, T0769, T0770, T0773, T0774, T0777, T0780, T0781, T0782, T0783, T0784, T0785, T0786, T0788, T0789, T0790, T0792, T0794, T0796, T0798, T0800, T0803, T0805, T0806, T0807, T0808, T0810, T0811, T0812, T0814, T0815, T0816, T0817, T0818, T0819, T0821, T0822, T0823, T0824, T0827, T0829, T0830, T0831, T0832, T0833, T0834, T0835, T0836, T0837, T0838, T0840, T0841, T0843, T0845, T0847, T0848, T0849, T0851, T0852, T0853, T0854, T0856, T0857, T0858
Total :	333 targets, 73,418 models

Table S6: CASP targets in the validation dataset.

Dataset	Targets
CASP12 39 targets 5,411 models	T0859, T0860, T0862, T0863, T0864, T0865, T0866, T0868, T0869, T0870, T0871, T0872, T0873, T0879, T0886, T0889, T0891, T0892, T0893, T0896, T0897, T0898, T0900, T0902, T0903, T0904, T0911, T0912, T0918, T0920, T0921, T0922, T0928, T0941, T0942, T0943, T0944, T0945, T0947
Total :	39 targets, 5,411 models

Table S7: CASP targets in the test dataset.

Dataset	Targets
CASP12 38 targets 5,471 models	T0859, T0860, T0862, T0863, T0864, T0866, T0868, T0869, T0870, T0871, T0872, T0873, T0879, T0886, T0889, T0891, T0892, T0893, T0896, T0897, T0898, T0900, T0902, T0903, T0904, T0911, T0912, T0918, T0920, T0921, T0922, T0928, T0941, T0942, T0943, T0944, T0945, T0947
CASP13 73 targets 10,882 models	T0954, T0955, T0957s1, T0957s2, T0958, T0959, T0960, T0961, T0962, T0963, T0964, T0965, T0966, T0967, T0968s1, T0968s2, T0969, T0970, T0971, T0973, T0974s1, T0974s2, T0975, T0976, T0977, T0978, T0979, T0980s1, T0980s2, T0982, T0983, T0984, T0985, T0986s1, T0986s2, T0987, T0989, T0990, T0991, T0992, T0993s1, T0993s2, T0995, T0996, T0997, T0998, T1000, T1001, T1002, T1003, T1004, T1005, T1006, T1008, T1009, T1010, T1011, T1013, T1014, T1015s1, T1015s2, T1016, T1017s1, T1017s2, T1018, T1019s1, T1019s2, T1020, T1021s1, T1021s2, T1021s3, T1022s1, T1022s2
Total :	117 targets, 16,353 models

References

[1] Kliment Olechnovič and Česlovas Venclovas. VoroMQA: Assessment of protein structure quality using interatomic contact areas. *Proteins: Structure, Function, and Bioinformatics*, 85(6):1131–1145, 2017.

[2] Ilia Igashov, Kliment Olechnovic, Maria Kadukova, Ceslovas Venclovas, and Sergei Grudinin. VoroCNN: Deep convolutional neural network built on 3D Voronoi tessellation of protein structures. *bioRxiv 2020.04.27.063586*, doi: https://doi.org/10.1101/2020.04.27.063586 2020.

[3] Mikhail Karasikov, Guillaume Pagès, and Sergei Grudinin. Smooth orientation-dependent scoring function for coarse-grained protein quality assessment. *Bioinformatics*, 35(16):2801–2808, 2019.

[4] Alexandre Hoffmann and Sergei Grudinin. NOLB: Nonlinear rigid block normal-mode analysis method. *Journal of chemical theory and computation*, 13(5):2123–2134, 2017.